Nat. Hazards Earth Syst. Sci. Discuss., https://doi.org/10.5194/nhess-2018-158
Manuscript under review for journal Nat. Hazards Earth Syst. Sci.
Discussion started: 29 June 2018

Natural Hazards and Earth System Sciences
Discussions

Flood depth estimation by means of high-resolution SAR images and LiDAR data

Fabio Cian[1], Mattia Marconcini[2], Pietro Ceccato[3], Carlo Giupponi[1]

[1]Department of Economics, University of Venice Ca' Foscari, Venice, 30121, Italy
[2]DFD German Aerospace Center (DFD-DLR), Wessling, 82234, Germany
[3]International Research Institute for Climate and Society (IRI), Columbia University, New York, USA

Correspondence to: Fabio Cian (fabio.cian@unive.it)

Abstract. When floods hit inhabited areas, great losses are usually registered both in terms of impacts on people (i.e., fatalities and injuries) as well as economic impacts on urban areas, commercial and productive sites, infrastructures and agriculture. To properly assess these, several parameters are needed among which flood depth is one of the most important as it governs the models used to compute damages in economic terms. This paper presents a simple yet effective semi-automatic approach for deriving very precise inundation depth. First, precise flood extent is derived employing a change detection approach based on the Normalized Difference Flood Index computed from high resolution Synthetic Aperture Radar imagery. Second, by means of a high-resolution Light Detection And Ranging Digital Elevation Model, water surface elevation is estimated through a statistical analysis of terrain elevation along the boundary lines of the identified flooded areas. Experimental results and quality assessment are given for the flood occurred in the Veneto region, North-Eastern Italy, in 2010. In particular, the method proved fast and robust and, compared to hydrodynamic models, it requires sensibly less input information.

1 Introduction

Climate science foresees a future where extreme weather events could happen with increased frequency and strength as a consequence of anthropogenic activities. Specifically, climate change would favour extreme precipitations, which could cause riverine, flash and coastal floods (i.e., the main source of losses in the world as reported by MunichRE (2014)) to occur more and more often. The higher probability of these events to happen is also exacerbated by land-use change and in particular, by settlement growth which increases soil sealing and, hence, water runoff. The ultimate consequence would be an increase of fatalities and injuries, but also of economic losses in urban areas, commercial and productive sites, infrastructures and agriculture.

Flood risk and impacts are not sufficiently understood and documented and need to be monitored systematically with improved precision as underlined by the European Flood Directive (European Commision, 2007). This is particularly important to support climate change adaptation policies, as well as to develop robust public disaster relief funds, risk profile for financial institutes, risk portfolio for re-insurance companies and risk in supply chain for multinational companies (Mysiak, 2013; UNISDR, 2015). In order to assess flood impacts, besides their extent, several other parameters shall be monitored during the event, such as flow velocity, debris factor and inundation depth. Here, flood depth is particularly important since it governs the damage functions (or vulnerability curves or loss functions), which define the expected loss given a certain flood depth (Mojtahed, 2013; Scorzini, 2015).

Therefore, in ex-post assessment deriving flood depth is essential to quantify impacts and damages, to better characterize flood risk, as well as to implement disaster risk reduction measures. Furthermore, it also has a key role in supporting emergency response, assessing accessibility and designing suitable intervention plans, calculating water volumes and allocating resources for water pumping, as well as rapidly estimating the costs for intervention and reconstruction.

In Veneto, North-Eastern Italy, several floods caused major damages in the past decade as the one occurred in 2010 in the city of Vicenza and its surroundings, which was the most serious in the area over the last 50 years (ARPAV, 2010). Moreover, extreme weather events are expected to increase in the future due to climate change (Zollo, Rillo, & Bucchignani, 2015) in the entire region, where therefore there is a great interest in monitoring floods.

To this purpose, remote sensing and in particular Synthetic Aperture Radar (SAR) data have been playing an important role since decades allowing, during crises, the derivation of flood extent maps like those provided by the European Copernicus Emergency Management Service (Copernicus EMS) or the International Charter on Space and Major Disaster (International Charter) (Martinis 2015). In fact, SAR sensors are particularly suitable for this task due to their capability of observing through clouds (thanks to microwaves all-weather capabilities) and during night (having their own source of illumination). Moreover, water surfaces are generally characterized by a very low backscattering (the portion of the outgoing radar signal that the target redirects directly back towards the radar antenna) due to the specular reflection of microwaves (O'Grady, Leblanc, & Gillieson, 2011), hence making water mapping relatively easy. SAR data at high spatial resolution are continuously acquired by many satellites in low Earth orbits, such as the German TerraSAR-X (TSX), the Italian COSMO-SkyMed (CSK) and more recently the ICEYE and the European Space Agency (ESA)'s Sentinel-1 (S1) constellations. These sensors can provide images up to a resolution of a fraction of a meter (e.g., TSX, CSK) and are able to promptly monitor disaster within few hours from their occurrence (e.g., CSK in urgent mode activation).

Several types of algorithms have been developed to map floods using SAR data. Among the most used, largely-employed thresholding techniques aim at identifying a backscattering value below which a pixel is categorized as water. Specifically, such threshold can be determined using automated procedures but it might consistently vary depending on e.g. environmental factors or the specific satellite acquisition geometry (Giustarini et al., 2015; Henry, 2006; Martinis, 2009; Pierdicca, 2013). Another very common solution relies on the use of change-detection techniques, which compute the difference between an image acquired during the flood and one acquired before the event. In particular, flooded areas can be identified as they are associated with a decrease in the backscattering. On the one hand, this allows to discriminate permanent water bodies (mostly characterized by low and stable backscattering values) from temporary water surfaces; on the other hand, it might occur that land-cover changes associated with different backscattering values at the two considered time steps (as typically occurs for crops) can lead to overestimation of flooded areas (Giustarini, 2015; Giustarini, 2013; Long, 2014; Matgen, 2007).

The abovementioned approaches generally fail to detect floods occurring in vegetated areas where the water surface is obscured by tree branches and leaves. This might become a critical issue in regions characterized by a large amount of woodland and medium to tall vegetation and requires users to be extra-vigilant to interpret the results. Furthermore, due to lack of details in medium/low resolution SAR data and to the multiple scattering and signal returns in high resolution images, mapping flood in urban areas may be very difficult if not impossible (Schumann et al., 2011).

A new methodology (Cian et al., 2018), developed by the authors and also used in this work for deriving flood maps, is based on the use of the Normalized Different Flood Index (NDFI). The index is based on the multi-temporal statistical analysis of two sets of images, one containing only the images before the event, and another one containing images both of the event and before the event. Through the computation of the NDFI, a change detection is performed, and flood maps are derived. The index highlights flooded areas and allows to easily separate flooded pixels by non-flooded ones by means of a constant threshold.

Once derived the flood extent, flood depth can be assessed using Digital Elevation Models (DEMs). In this context, several approaches have been developed in the past yet from the 1980s. Gupta & Banerji (1985) used 60m spatial resolution Landsat Multispectral Scanning System (MSS) imagery to derive the water volume of a dam reservoir in the Himalayas and estimated the water level superimposing the boundary line of the water surface to a topographic map. Ten years later, Oberstadler et al. (1996) employed 12.5m resolution ERS-1 data for outlining the flood extent and overlaid the resulting map

Nat. Hazards Earth Syst. Sci. Discuss., https://doi.org/10.5194/nhess-2018-158
Manuscript under review for journal Nat. Hazards Earth Syst. Sci.
Discussion started: 29 June 2018

plotted with transparency to a map with topographic contours; next, water levels were manually registered at 500 m steps. Mason et al. (2001) derived the inter-tidal shoreline with ERS SAR data and estimated its height using a model based on depth-averaged hydrodynamics including the effects of tides and meteorological forcing. Matgen et al. (2007) used ENVISAT-ASAR multitemporal scenes and a Light Detection And Ranging (LiDAR) DEM (at 12.5m and 2m resolution, respectively) to derive the water depth for the 2003 flood of the Alzette river in Luxembourg. Specifically, flood edges obtained from ASAR imagery were intersected with LiDAR data to estimate the elevation at the boundary line of water polygons. In particular, the water surface was computed using two different interpolation modeling: Triangulated Irregular Network (TIN) generation and multiple linear regression; then, the depth was calculated subtracting the DEM to the water elevation. This study was further improved by Schumann et al. (2007) where the authors retrieved the water elevation combining the regression model with the TIN generation. Furthermore, the same methodology was also employed by Schumann et al. (2008) to compare the results obtained using different elevation information, namely topographic contours, Shuttle Radar Topographic Mission (SRTM) DEM and LiDAR-based DEM. Best results were obtained with 2m resolution LiDAR data but good performances could be achieved even with the 90m resolution SRTM DEM. Zwenzner & Voigt (2008) proposed a similar technique based on a model fitting the water elevation separately derived for the left and right riverbanks by combining the flood extent estimated from SAR data with DEM data. Here, to estimate the water level a sequence of densely spaced river cross sections is shifted and adjusted individually.

All abovementioned approaches assume that the water level during the flood event is the same at both sides of the river cross section, thus assuming that the riverbanks are perfectly symmetric and that river flow and floodplain dynamics are not conditioning the overflow and the following stream. Nevertheless, while this hypothesis accounts for the river slope and defines an equilibrium condition at the ends of the cross-section (i.e., they exhibit the same elevation), it may actually not fit many types of floods caused e.g. by riverbanks ruptures, asymmetric river banks or complex inundation dynamics.

More recently, Huang et al. (2014) derived flood depth by combining Landsat and LiDAR data under the assumption that the water plane can be considered flat if the flooded area is sufficiently small. Accordingly, they split the flood extent map obtained from Landsat data into 750x750m squared tiles. Then, for each of them they "filled" the LiDAR DEM up to the level for which the resulting water extent was closest to the Landsat-based map (measured in terms of Kappa coefficient (Cohen, 1968)). For tiles completely covered by water, the average height of the 8 neighbour tiles is taken. Finally, the water surface is calculated using an interpolation method (i.e., Kriging) and the depth computed as the difference with respect to the DEM. A similar approach was also presented by Matgen et al. (2016). Brown et al. (2016) derived a flood extent map from SAR using a semi-automated method (thresholding, manual interpretation and correction). At 100-m intervals, elevation values along the flood edges were detected by means of a LiDAR. Elevation points were inspected, in certain cases corrected or added manually by an operator, in order to improve the water surface elevation estimation. The water surface was then created using TIN interpolation.

Instead, Iervolino et al. (2015) describes a model of SAR backscattering in case of flood (post-event) and in case of no flood (pre-event). From the inversion of the model and the comparison between pre- and post-event condition, they derive the flood depth. They propose two methods: i) "Single Image Object Aware", which allows to estimate the level of the water next to a building whose characteristics must be known (*i.e.* Object Aware), given that two gauges' measurements are available in its premises; and ii) "Two Images Areas Aware", which uses a pre-event and a during/post-event image to retrieve the water levels for the whole area, using an unflooded area in the during/post-event image for calibration (*i.e.* Area Aware). Even though an interesting and promising approach, the two methods look complex and difficult to be implemented. Furthermore, ancillary data of difficult retrieval are needed, such as data from gauge stations and information about building affected by the flood.

As already mentioned, flood depth is important not only for emergency response, but also for impact assessment. Purely economic works use flood depth (usually retrieved from third parties) for assessing direct and indirect impacts of floods by

Nat. Hazards Earth Syst. Sci. Discuss., https://doi.org/10.5194/nhess-2018-158
Manuscript under review for journal Nat. Hazards Earth Syst. Sci.
Discussion started: 29 June 2018

Natural Hazards and Earth System Sciences
Discussions

means of depth-damage functions. However, if flood depth information is not available often the whole range of possible values is taken into account, hence resulting in extremely different scenarios. As an example, in Carrera et al. (2013) for a quite vast event (1182 Km^2) spreading all over northern Italy a range in the depth from 1 to 6m resulted in a damage estimate varying from 4 billion € to roughly 10 billion €. In a similar work, Amadio et al. (2016) could obtain better estimate of the losses caused by the 2014 flood in Emilia Romagna, Italy, employing a simulated maximum flood depth computed by D'Alpaos et al. (2014) by means of hydraulic models. Nevertheless, this required several input information, as well as high processing power.

In this paper, a new methodology is proposed for rapid computation of flood depth by means of SAR data and high-resolution DEM. Firstly, a flood map is derived from SAR data using the algorithm proposed in (Cian et al., 2018). Secondly, a statistical analysis is performed on the terrain elevation values detected on the boundary lines of the flooded polygon, to estimate the correct water elevation, needed to compute the flood depth. The hypothesis is that all the detected water surfaces are flat and theoretically showing a constant elevation value along their boundaries. As explained in detail in the methodology section, several sources of error make these values non-constant and the statistical analysis is a key step to estimate the correct water elevation.

The objective of this work is to present a semi-automatic, fast and reliable method to estimate a precise flood depth in support of economic impact assessment methods for a rapid estimation of losses (and precise in case of high-resolution elevation data available) as well as the development of emergency plans.

In Section 2 the proposed methodology is given. Section 3 describes the data used in the experimental analysis and the investigated study area, while Section 4 presents the results obtained. In Section 5 quality assessment and discussion are reported, whereas Conclusions are drawn in Section 6.

2 Methodology

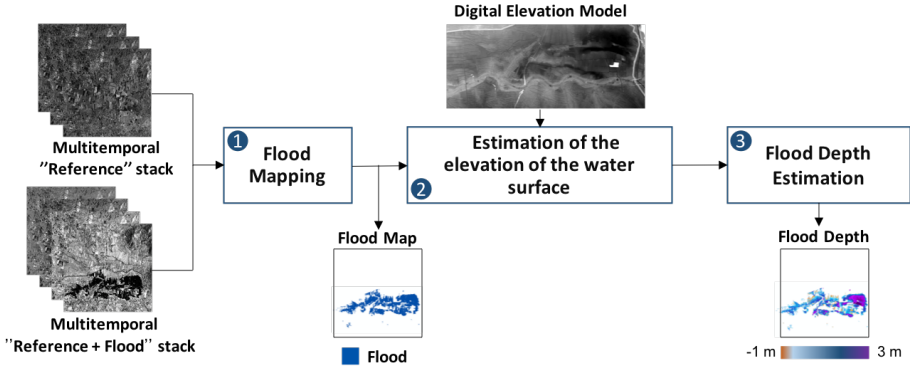

Figure 1 Flood Depth Estimation Methodology: 1) flood maps are derived using the methodology presented in Cian et al. (2018); 2) by means of a high resolution Digital Elevation Model the elevation of the water surface is estimated, through a statistical analysis of elevation values along the boundary line of each flooded area; 3) flood depth is computed by subtracting the elevation values to the estimated elevation of water surface

The novel methodology proposed for estimating flood depth is composed of three main steps, namely i) flood mapping (extent estimation), ii) water surface elevation estimation and iii) flood depth estimation. They are explained in detail in the flowing three subsections.

Nat. Hazards Earth Syst. Sci. Discuss., https://doi.org/10.5194/nhess-2018-158
Manuscript under review for journal Nat. Hazards Earth Syst. Sci.
Discussion started: 29 June 2018

2.1 Flood mapping

Flood mapping (block 1 in Figure 1) is based on the use of the Normalized Different Flood Index developed by the authors and explained in details in (Cian et al., 2018). The method is based on the multi-temporal statistical analysis of two stacks of SAR images: one containing only images before the flood, i.e. reference images ("Reference" stack) and another one containing reference images and images of the event ("Reference + flood" stack). The mean temporal backscattering for each pixel throughout the "Reference stack" is computed together with the minimum backscattering value of each pixel throughout the "Reference + flood" stack. The two statistics are used to derive the new Normalized Difference Flood Index (NDFI), which is the normalized difference between the mean(reference) and the minimum(reference + flood) value. The computation of the NDFI corresponds to a change detection step. In fact, the index highlights flooded areas and allows to easily separate flooded pixels by non-flooded ones by means of a constant threshold.

Therefore, in this step of the proposed system, after the computation of temporal statistics and of the NDFI index, a constant threshold on the NDFI value is applied (NDFI = 0.7) to extract flooded areas. Following the methodology presented in (Cian et al., 2018), three steps of post-processing are applied to the resulting flood maps to reduce the effect of speckle and to reduce spurious flooded areas: i) application of morphological filters (dilate and closing filter with a 3 by 3 pixels windows); ii) exclusion of clusters smaller than 10 pixels; iii) exclusion of the pixels falling in a slope of>5° (where a flood would be unlikely). The final flood maps are used as input of block 2 (Figure 1).

2.2 Water surface elevation estimation

In this step, we take as input the flood map previously generated and a high-resolution DEM of the area affected by the flood. The flood map is used to extract the boundaries of each flooded polygons to perform a statistical analysis of their elevation values by means of the DEM. Despite any DEM can be used in this methodology, it should exhibit a resolution of a fraction of a meter to obtain significant flood depth values for economic impact assessment.

The objective of this step is to estimate the elevation of the water surface for each detected flooded polygon, analysing the DEM elevation they exhibit along their boundaries. Similarly to Huang et al. (2014) and Brown et al. (2016), we suppose that the water surface of the flooded areas is flat. This can be considered a fair assumption in those cases where the slope of the affected area is gentle, and the velocity of the flood stream is modest. More precisely, we do not assume a single constant elevation value for the whole flood map, but a constant water elevation inside each detected flooded polygon, which thus allows taking into consideration the usual decrease of the water surface elevation along a river. Under this assumption, each polygon shall then exhibit a constant DEM elevation along its boundary, which corresponds to the elevation of the entire water surface contained in the polygon itself; nevertheless, this is not happening due to different error sources.

Nat. Hazards Earth Syst. Sci. Discuss., https://doi.org/10.5194/nhess-2018-158
Manuscript under review for journal Nat. Hazards Earth Syst. Sci.
Discussion started: 29 June 2018

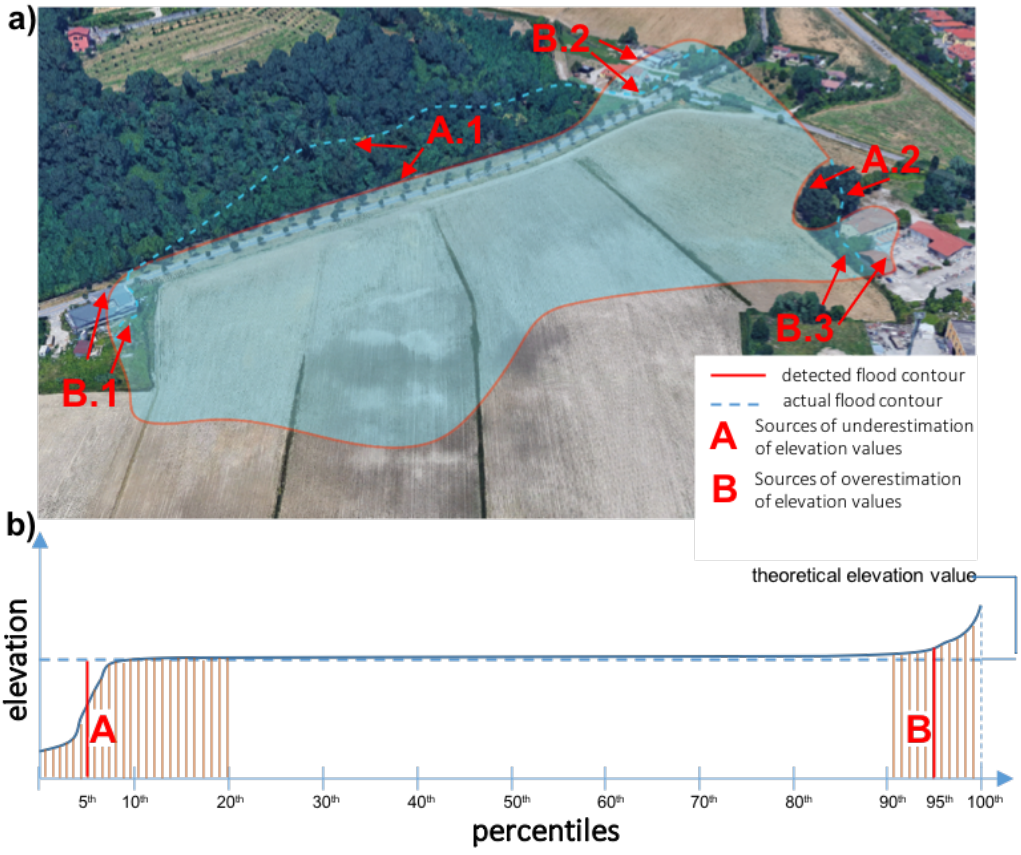

Figure 2 a) Example of a detected flood polygon (light blue transparency) and relative flood boundary (red line). The dashed light blue line indicates the actual flood boundary, not correctly detected by the SAR-based flood map due to presence of vegetation obscuring the flood (cases indicated by letter A) or due to radar shadow (cases indicated by letter B). In the errors indicated by A, the elevation values detected are lower than the actual ones. Vice-versa, in the errors indicated by B, the elevation values detected are higher than the actual ones. b) Plot depicting the distribution function of the elevation along the boundary (red line). Areas indicated with A and B represent the values associated to the errors as explained above. The two threshold values (at the 5th and the 95th percentiles) are used to exclude outliers.

Figure 2(a) shows an example of a detected flooded polygon (light blue transparency). Based on our theoretical assumptions, this water surface should have a constant elevation. In practice, this may not happen due to some sources of error (Figure 2(a)). Specifically, the detected flood boundary (red line) may not correspond to the real boundary of the flood (dashed light blue line) due to: A) vegetation obscuring flooded areas leading to omission errors, and B) the nature of SAR images (speckle, radar shadow, layover (Franceschetti & Lunari, 2018)) that can lead to false alarms or omission errors. Uncertainties in the SAR-based flood map, errors in the DEM and misalignment between the SAR data and the DEM can lead to further uncertainty in the detection of elevation values along the boundary lines, resulting in outlier values under- or overestimating the real water elevation value. The plot reported in Figure 2(b) shows the distribution (percentiles) of the DEM elevation values along the boundary lines. The above-mentioned errors (over- or/and underestimation) can be associated to the values contained in areas A and B. It is more likely to find outliers on the lower end of the elevation value distribution, since an underestimation is more likely due the sources of error abovementioned.

Nat. Hazards Earth Syst. Sci. Discuss., https://doi.org/10.5194/nhess-2018-158
Manuscript under review for journal Nat. Hazards Earth Syst. Sci.
Discussion started: 29 June 2018

Therefore, if we want to reliably estimate the correct water elevation for each flooded polygon, we need to identify and exclude outliers associated with omission errors (e.g. flood covered by vegetation), to commission errors (e.g. radar shadow included in the flood map) or misalignments between SAR and DEM data.

First, elevation values are extracted from the available input DEM in correspondence to the boundary of each flooded polygon individually. Then, the corresponding percentiles are computed (i.e., where a percentile denotes the value below which a given percentage of observations falls in the investigated group of observations) and values below the 5th and above the 95th percentile are removed since, from extensive experimental analysis, this generally proved rather effective for removing under- and overestimation errors.

Next, given our hypothesis of a flat water surface, we have to check if the elevation value distribution is stable. Knowing that locally we can find a non-stable distribution (due to the abovementioned sources of error), starting from n=95 we iteratively compute, with step 1, the difference between the DEM value corresponding to the n^{th} and the $(n-5)^{th}$ percentile, respectively. If the difference is greater than 10 cm, then the process continues; otherwise we stop and compute the water elevation as the mean value between the extremes of the 5-percentile interval analysed at the last iteration. The idea is to identify a plateau in the distribution that can represent the correct water elevation.

We start looking for the correct elevation from the high-end of the distribution for two reasons: i) statistically there are less outliers on this side of the distribution and ii) because it is the highest correct value of water elevation that determines the overall water elevation for the considered flooded polygon. The 95th percentile represents a good starting point, able in most cases to exclude all the outliers present in one single polygon.

A step of five percentiles was found to be an optimal indicator of stability compared to the comparison of consecutive percentiles. This adaptive threshold takes care of the different conditions of each single polygon and allows increasing the precision of the method. As expected, the statistical distribution of elevation values is not identical for each boundary line. Therefore, a fixed threshold would have led to and increased uncertainty in the final water surface elevation estimation, especially in those cases where flood polygons have a non-regular geometry, which can overlap a complex topography or can encompass vegetation, roads, built-up areas.

A threshold check is set on the 50th percentile, allowing us to spot possible wrong estimations. In fact, an elevation of the water surface below the 50th percentile is indicating an exceptional behaviour of the analysed boundary line, which would need dedicated investigation.

The water surface elevation estimation step is carried out using a Python^{TM} script including the *arcpy* library (ArcPy). In this script, we provide as inputs the flood map (shapefile format) and the DEM (raster format). The DEM is clipped using the boundary line of a flood polygon by means of the *arcpy* function *ExtractByMask*. Then, the elevation values of this newly created raster are analysed and their distribution (percentiles) is computed. The procedure is repeated for each flooded polygon in the flood map and the distribution values of each polygon are added in the attribute table of the shapefile. Finally, the algorithm selecting the optimal water elevation value is summarized by the following:

$n = 95$
for $i = 0$ *to* $(n-5)$
  if $[P_{n-i} - P_{(n-5)-i}] \leq 10$ *cm then*
    Water Surface Elevation $= [P_{n-i} + P_{(n-5)-i}] / 2$
    Else
      $i = i + 1$
  endif
if $(n-5-i) = 50$ *then warning*

Nat. Hazards Earth Syst. Sci. Discuss., https://doi.org/10.5194/nhess-2018-158
Manuscript under review for journal Nat. Hazards Earth Syst. Sci.
Discussion started: 29 June 2018

endfor

with P indicating the percentile and n the upper percentile threshold.

2.3 Flood depth estimation

Finally, depth is determined for each flooded pixel as the difference between its DEM value and the water elevation estimated for the corresponding flooded polygon.

In few cases, where the polygon geometry or the topography is non-regular, the estimation of the water level can be unprecise. However, if this is not yet detected by the threshold check, it can be easily detectable by analysing at the resulting flood depth values. If, inside a given polygon several negative values are obtained, this indicates an underestimation of the water elevation. Instead, if a given pixel is associated with a flood depth much higher than its neighbours, then the water level may have been overestimated. Therefore, we select the polygons showing unexpected behaviours and we compare them with a DEM-fill approach. The DEM is filled up to the estimated water surface elevation. If the resulting polygon extent does not match with the observed flooded polygon, we manually look for the elevation value that best approximated the flood extent and set it as the water elevation. Then we compute again the flood depth and reiterate the steps until we have a satisfying result.

3 Data Used and Case Study

3.1 Veneto Flood 2010

From October 31 to November 2, 2010, in the Veneto Region, North-East Italy, 140 km^2 of land have been flooded with major damages on properties and infrastructures. The event was originated by an Atlantic perturbation, which caused intense precipitation over the whole area, with extremes in the pre-alps and piedmont areas. Local rainfall accumulation exceeded 500 mm and the average widely surpassed 300 mm, leading to a serious hydraulic stress, especially in the area of Vicenza and the south of Padua. Sirocco wind, persistent on sea and inland, slowed the discharge of rivers into the sea. Early snow melted due to the warm temperature also added water to the rainfall.

The first rupture in the study region occurred south of Vicenza in the afternoon of November 1. The flood then propagated southwards until Veggiano, where the banks of the Bacchiglione river were broken during the night between November 1 and 2 in the areas of Bovolenta and Saletto (see Figure 3). Overall 262 municipalities were affected leading to roughly half billion Euros damage, three fatalities, 3500 displaced and more the 500 thousand people affected. The flood also triggered hundreds of landslides in the mountainous surroundings, which led to more than 500 warnings of instability phenomena received by the province soil protection division (Floris et al., 2012; Scorzini, 2015). This paper analyses three main areas as shown in Figure 3: Vicenza and its surrounding (A), the Bovolenta area at the south of Padua (B) and the Saletto area at the south of Colli Euganei (a group of hills of volcanic origin that rise to heights of 300 to 600 m a few km south of Padua) (C).

Nat. Hazards Earth Syst. Sci. Discuss., https://doi.org/10.5194/nhess-2018-158
Manuscript under review for journal Nat. Hazards Earth Syst. Sci.
Discussion started: 29 June 2018

Natural Hazards and Earth System Sciences
Discussions

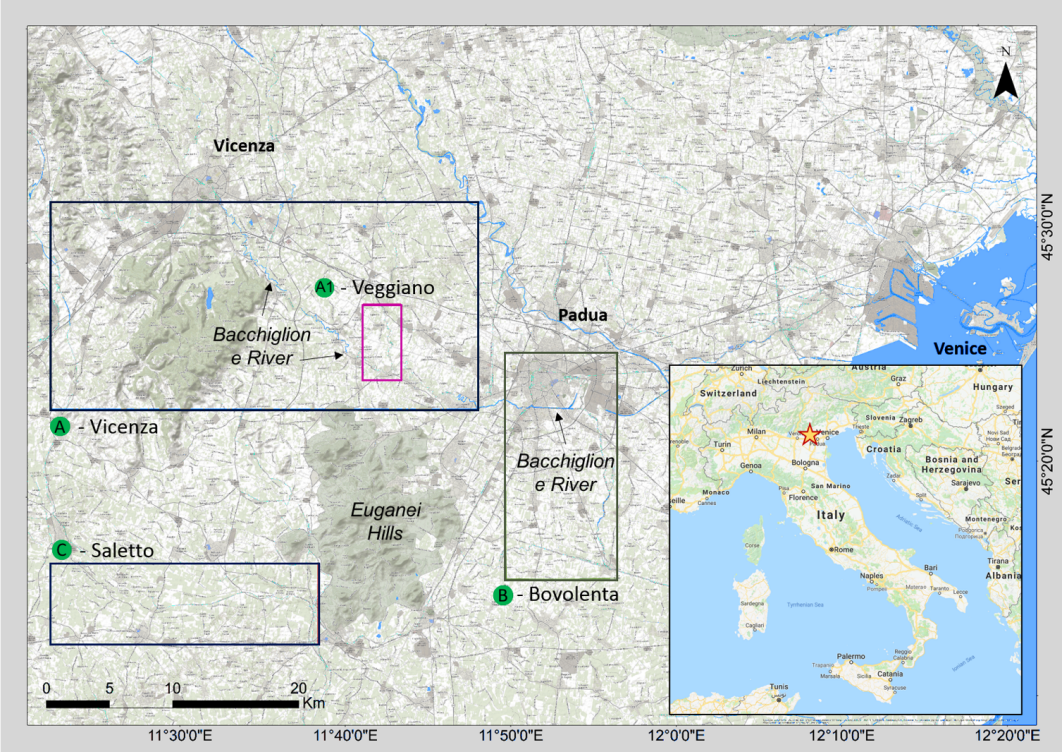

265 **Figure 3 Overview of the area affected by the flood of 2010, Veneto region, Italy. The three main areas of interests are highlighted: A) Vicenza, B) Bovolenta and C) Saletto. Area A1) refers to Veggiano area covered by the hydrodynamic modeling used as an assessment dataset.**

3.2 Data Used

Flood maps were derived using CSK data, provided by the Italian Space Agency, following the methodology proposed
270 by Cian et al. (2018). Table 1 reports the complete list of scenes used.

Table 1 List of COSMO-SkyMed SAR data (Stripmap 3 m) used for deriving flood maps of the event

Date	Status	Acquisition Time (UTC)
31/Oct/2008	Reference	17:35
28/Apr/2010	Reference	17:30
29/Aug/2010	Reference	5:01
01/Nov/2010	Flood	5:01
03/ Nov /2010	Flood	17:22
04/ Nov /2010	Flood	18:10
06/ Nov /2010	Flood	17:28
07/ Nov /2010	Flood	5:13

Additionally, different DEMs were used for estimating the flood depth:

275 - the LiDAR Digital Terrain Model (DTM) from the Venice River Basin Authority at 2m resolution produced in 2004, which was employed for the Vicenza area of interest;

- the LiDAR DTM from the ministry of Environment at 1m resolution produced in 2012, which has been used for the areas of Bovolenta and Saletto;
- the 5m resolution DTM at 5 available from the Veneto Region geodatabase, which was used for the whole area of interest for the cross-comparison with the hydrodynamic model.

To validate the results, in absence of proper ground truth, we made use of different datasets that allowed us a qualitative assessment of our maps:

- A simulation of the event by means of a hydrodynamic model, where flood extent was estimated for November 3 and 4 using the 2DEF finite elements model (Viero et al., 2014) and flood depth was obtained as described by Viero et al. (2013). The simulation was computed in order to correspond to the exact moment of the SAR acquisition and it was performed using the DTM of the Veneto Region at 5 m resolution;
- A set of aerial photographs acquired on November 1 taken by the Firemen Department of Vicenza covering mainly the Vicenza area of interest;
- A set of in situ photographs taken from the Civil Protection on November 1 and 2 covering the area of Saletto.
- A set of in situ photographs taken by the authors in 2017.

4 Results

4.1 Elevation values distribution

As discussed above, the proposed methodology is based on the statistical analysis of the elevation values along the boundary lines of the estimated flooded polygons. Figure 4 shows the distribution (percentiles) of elevation values for 18 randomly selected polygons in the Vicenza area of interest on November 3. As discussed in Section 2, on the tails of the distribution (below the 5th and above the 95th percentile) we can notice some irregularities, i.e. non-flat profiles, in contrast to more stable behaviours in most of the cases in the central part of the profiles. The thresholds on the 5th and 95th percentile cut out most of the outliers. By means of the adaptive threshold starting from the 95th percentile, the method is able to estimate the elevation of the water surface looking for a plateau on the distribution. It prevents to overestimate water elevation since it gets rid of upper outliers, it prevents to underestimate it posing a limit on the lower percentile and setting a condition on the slope of the profile (elevation difference equal or lower than 10 cm in a step of five percentiles). Less regular profiles can be seen in the plot, like the one indicated by the arrows A and B in Figure 4. The irregularity is due to errors in the flood map, such as the case when vegetation obscures part of the flooded area, when there is a misalignment between the flood map and the DEM, when flooded polygons exhibit a non regular geometry or when the DEM along the flood boundaries has a complex topography. In these cases (less than 3%), the proposed methodology might not result in reliable estimations. In fact, the elevation can exhibit two problems: i) it never shows a stable value along the distribution (no plateau is found) and the water elevation is associated with the 50th percentile; and ii) it presents a plateau at a higher elevation with respect to the real water surface elevation, resulting in an overestimation of the flood depth (this may rarely happen for example when the flood map crosses over roads or river banks at higher elevation due to inaccuracies of the flood map or misalignment between the flood maps and the DEM). The threshold check set at the 50th percentile detects the first problem, while the second is detected by looking at high value of flood depth (> 2m) or by finding discontinuities between neighbouring polygons in the estimated surface water elevation. For those few cases, it is necessary to intervene manually as it is not possible to estimate the right elevation simply looking at this statistic, as described at the end of Section 2.

Nat. Hazards Earth Syst. Sci. Discuss., https://doi.org/10.5194/nhess-2018-158
Manuscript under review for journal Nat. Hazards Earth Syst. Sci.
Discussion started: 29 June 2018

Natural Hazards and Earth System Sciences
Discussions

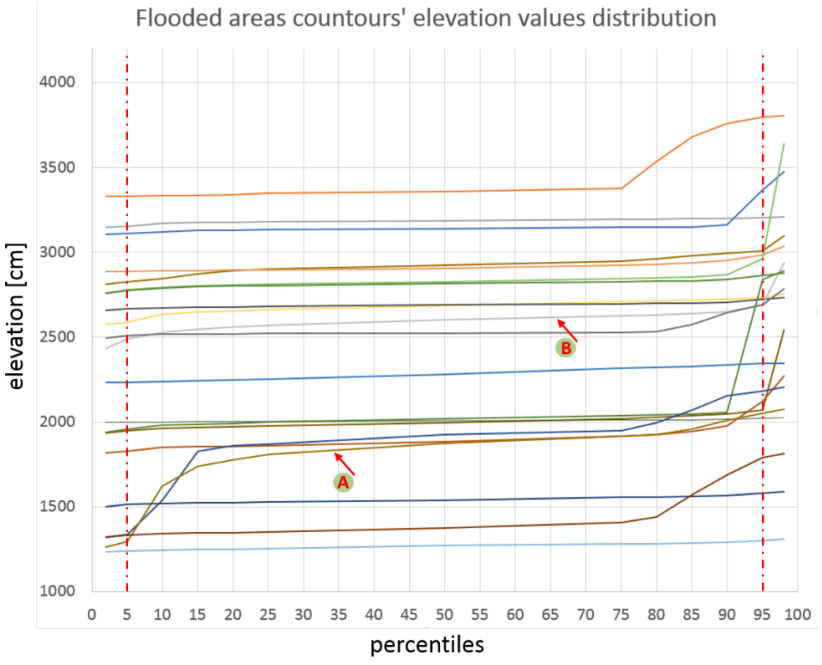

315 **Figure 4 Elevation values distribution (percentiles) for a random selection of flood polygon's boundaries in the Vicenza area on November 3. The 95th and 5th percentile thresholds are highlighted. Arrows "A" and "B" indicate less regular profiles, for which the proposed methodology is less effective. In these cases (less than 3% of the total) it is necessary a manual intervention.**

4.2 Flood Depth Estimation

Flood depth was computed for the three areas of interest indicated in Figure 3. Flood depth was estimated for the whole
320 flooded area except for a small portion of Veggiano area (a portion of the A.1 area indicated in Figure 3), where LiDAR data was not available. Figure 5 shows the results for the Vicenza area of interest. Specifically, Figure 5(a) shows the flood maps for November 3 and 5(b) the LiDAR extent, which covers the entire flood with the exception of the central part of the map (the portion of the Veggiano area mentioned above). Figure 5(c) and 5(e) show respectively water surface elevation and flood depth for November 3. Figure 5(d) and (f) show water surface elevation and flood depth for November 4. The dynamics of the
325 event, i.e. the receding of water from November 3 to 4, can be noticed where extent and depth of the flood decrease. The flooded area extends for several kilometers along the Bacchiglione river where the terrain elevation decreases gradually from the north-west to the south-east. Since we estimate water elevation for each single polygon, we are able to take into consideration also the slope of the river. This can be noted in the overall decreasing of water surface elevation values in Figure 5(c) and (d).

330 For types of floods similar to this, the hypothesis of a flat water surface inside a single polygon is a good approximation since the flood evolution is slow and therefore water surface can be considered flat. This is especially true in case of the Bovolenta and Saletto area of interest where the flood extent was limited and the topography relatively simple.

Figure 6 shows the flood depth for the Bovolenta area of interest on (a) November 4 and (c) 6. Also in this case, we can notice the receding of flood extent between the two dates. Figure 6(b) and (d) show a zoom of the results where the high level
335 of detail can be appreciated.

Figure 7 shows the results for the Saletto area of interest on (a) November 3, (b) 4, (c) 6 and (d) 7. In this case, the evolution of the event, in particular the decrease of flood extent and depth is even clearer given the higher number of observations available.

Nat. Hazards Earth Syst. Sci. Discuss., https://doi.org/10.5194/nhess-2018-158
Manuscript under review for journal Nat. Hazards Earth Syst. Sci.
Discussion started: 29 June 2018

Natural Hazards and Earth System Sciences
Discussions

As it is evident from the depth maps and the relative scales, there can be negative values of flood depth, which in most of the cases occur at the proximity of the boundaries of flooded polygons. These indicate most likely an underestimation of the water surface elevation, even if also false alarms in the flood map can induce to the same problem. However, the negative values are in most of the case in the order of few centimeters (less than 10 cm) and these pixels can be considered as very shallow water.

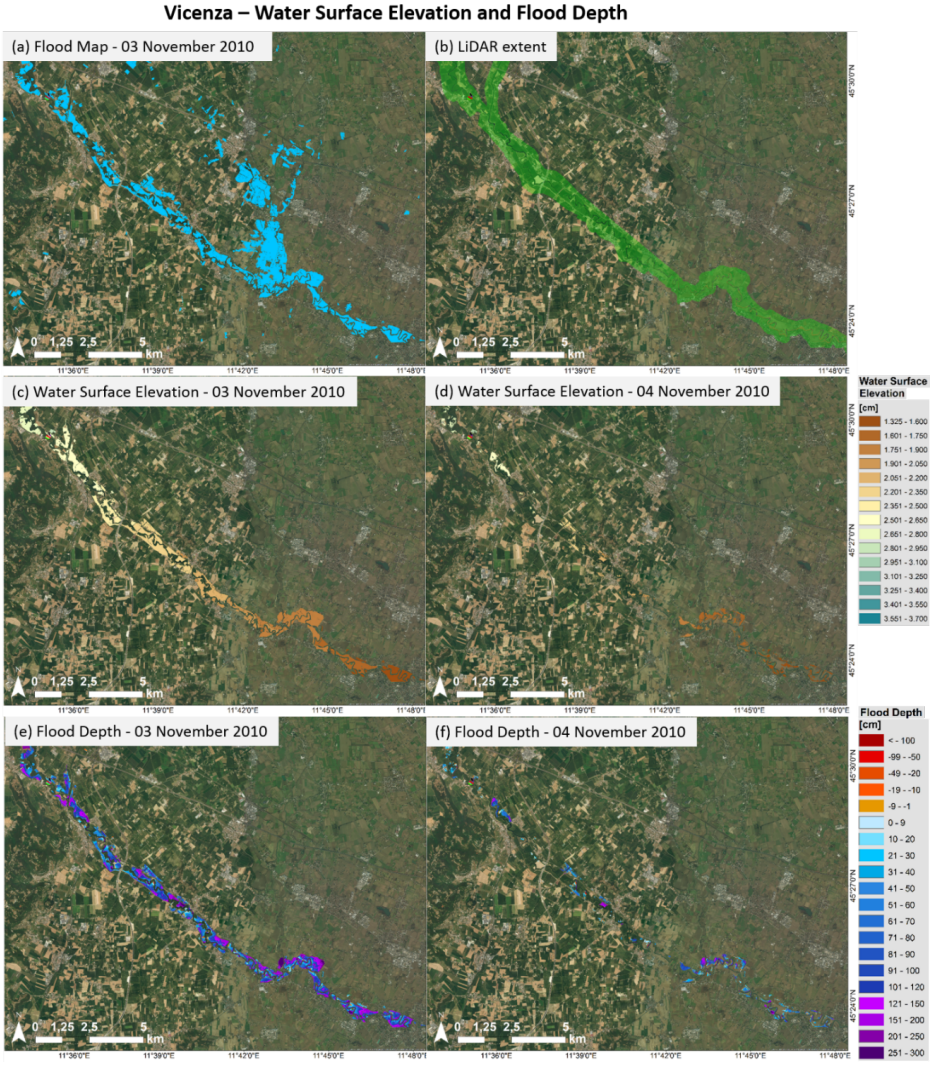

Figure 5 Water Surface Elevation and Flood Depth estimation for Vicenza area of interest on November 3 and 4. (a) shows the flood map for November 3 and (b) the extent of the LiDAR data, which does not completely cover the flooded areas. (c) and (d) show water surface elevation, (e) and (f) show flood depth, respectively for November 3 and 4. Reddish values in (e) and (f) indicate negative flood depth, therefore an error in the estimation of the water surface elevation (underestimation).

Nat. Hazards Earth Syst. Sci. Discuss., https://doi.org/10.5194/nhess-2018-158
Manuscript under review for journal Nat. Hazards Earth Syst. Sci.
Discussion started: 29 June 2018

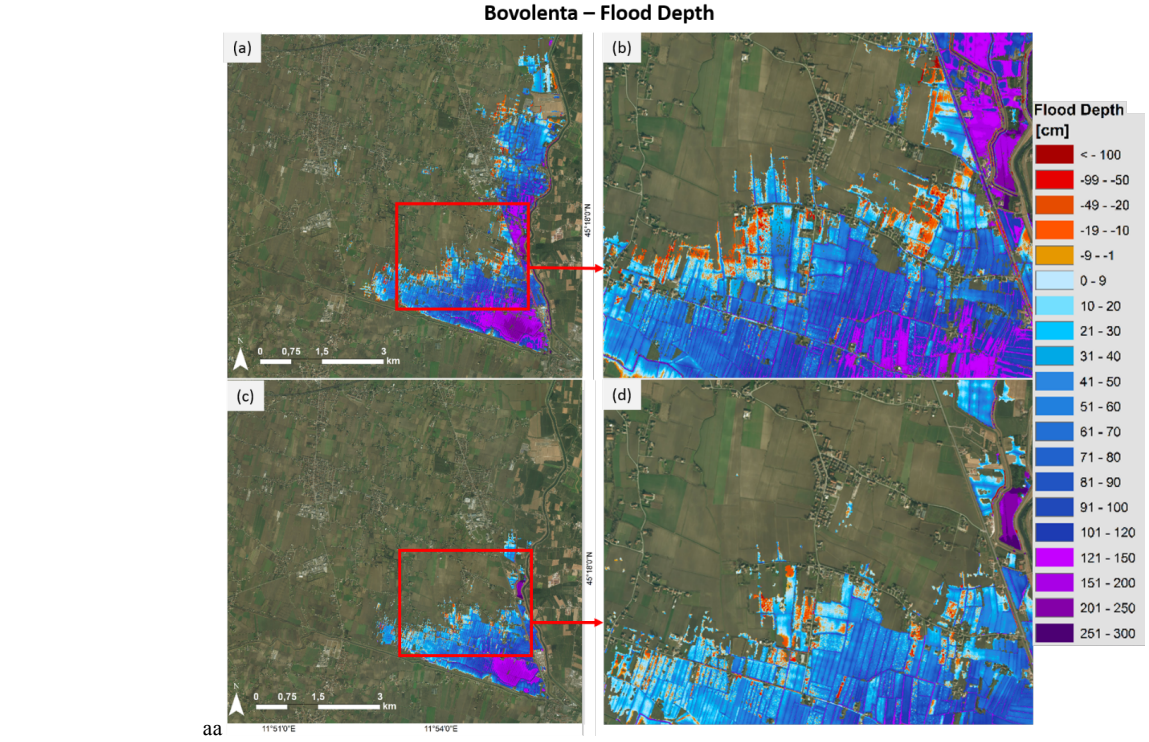

aa

Figure 6 Flood Depth for the Bovolenta area of study on (a) November 4, and (c) November 6. (b) and (d) show a zoom of the results highlighting the high level of detail achievable. Reddish pixels represent the error in the water level estimation.

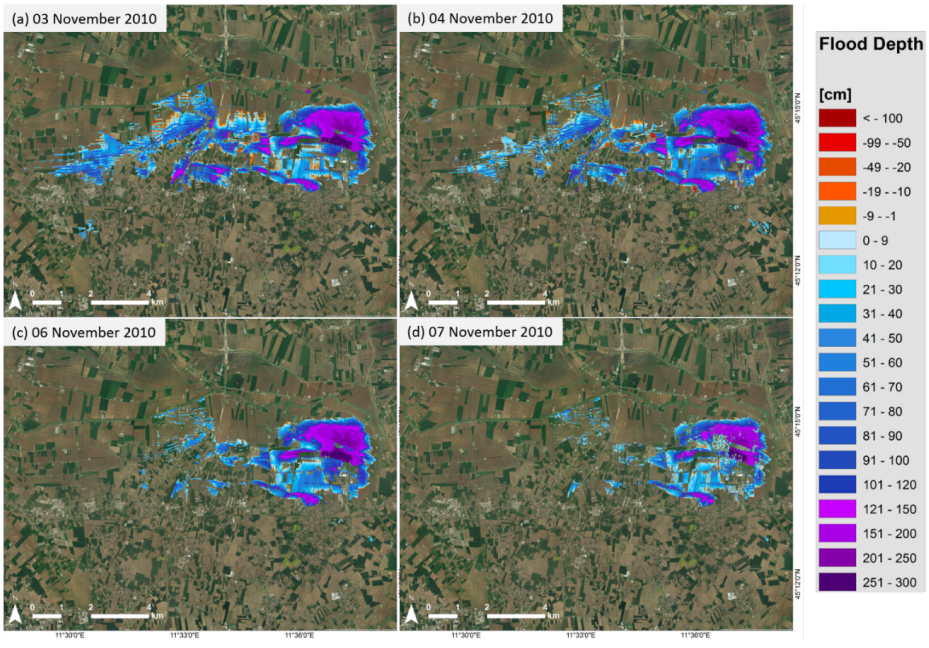

Figure 7 Flood Depth for the area of interest of Saletto on (a) November 3, (b) 4, (c) 6 and (d) 7

Nat. Hazards Earth Syst. Sci. Discuss., https://doi.org/10.5194/nhess-2018-158
Manuscript under review for journal Nat. Hazards Earth Syst. Sci.
Discussion started: 29 June 2018

Natural Hazards and Earth System Sciences
Discussions

355 **5 Assessment and Discussions**

5.1 Assessment with Aerial Photos

Ground truth data consist of aerial photographs taken on November 1 right after the beginning of the event, and of field pictures taken on November 1 and 2 by civil protection. Unfortunately, they do not match the dates and time of satellite acquisitions, therefore they cannot be used as a proper validation dataset. However, given the slow dynamic of the flood, they
360 can provide very useful information about the water level, which can be estimated and compared with the results of our method and therefore provide an assessment of the results. To prove this, in Figure 8 we show a comparison of flood extents derived for November 2 from 25m resolution Radarsat-2 data, and for November 3 from 5m resolution CSK imagery. The lower resolution of Radarsat-2 does not allow extracting the same level of detail of the map based on CSK data, but it is enough to show that the status of the flooded areas in the two consecutive days is very similar. Therefore, it makes sense to use the
365 available aerial photographs for assessing the results, keeping in mind a possible change in the flood status between the two situations. In particular, from the image we can notice that for the Vicenza area (Fig. 8a and 8b) the flood has receded from November 2 to 3, while for the Saletto area (Fig. 8c and 8d) it has expanded.

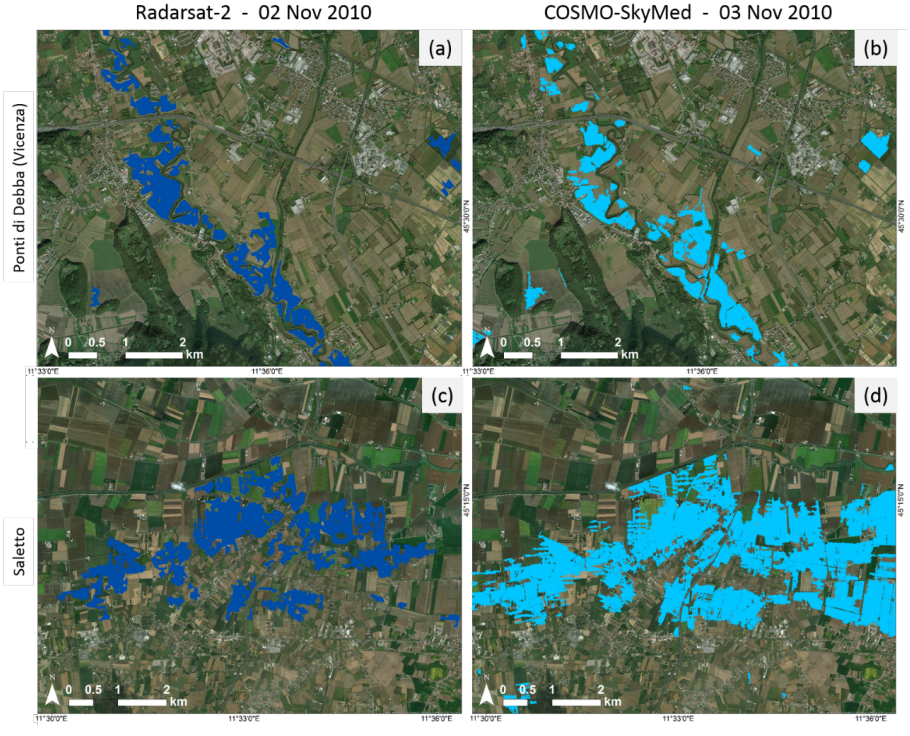

Figure 8 Comparison between Radarsat-2- (November 2, 2010) and COSMO-SkyMed-based flood maps (November 3, 2010). Radarsat-2 has a lower resolution (25 m) compared to COSMO-SkyMed (5 m), which provides a coarser flood map. Wan see by the comparison of the two maps that the flood has comparable extent in the two days. In particular, from the image we can notice that for the Vicenza area (Fig. 8a and 8b) the flood has receded from November 2 to 3, while for the Saletto area (Fig. 8c and 8d) it has expanded.

The assessment is carried out in three different steps: 1) estimation of water elevation corresponding to the dates of the
370 aerial photos acquisition; 2) analysis of water elevation obtained using the proposed SAR-based method; and 3) cross-comparison of the two values.

Concerning step 1, we made use of i) a DEM-fill technique and ii) of data acquired during a fieldwork of late 2017. DEM-fill consists of "filling" the DEM up to the elevation that gives a flood extent similar to the one displayed by the photos, which will be the estimated water elevation. In the fieldwork, we measured the height of the water plane on features recognizable in the aerial photos. These measurements added to the DEM value in the same location, allows the estimation of water elevation. Averaging these two values allows the estimation of the water elevation at the moment of acquisition of the aerial photos, which can be compared with the results given by the proposed SAR-based method.

Concerning step 2, SAR-based results are analysed in comparison with a DEM-fill method to understand the consistence of flood depth values in relation to the extent of DEM-based simulated flood.

Concerning step 3, the cross-comparison is done by comparing water elevation obtained in step 1 and 2.

The assessment was performed for the flood depth maps of November 3, the date of the first high resolution SAR image available after the acquisition of the aerial photos.

In **Panel I** of Fig. 9, Figure 9(a) shows flood extent and depth on November 3 at 17:22 UTC on the area of Ponti di Debba, south of the city of Vicenza, derived from the CSK SAR image shown in Fig. 9(b). **Panel II** of Fig. 9 shows aerial photo and fieldwork of the same area. Fig. 9(c) shows the aerial photo acquired on November 1 at 14:00 UTC, where three areas are highlighted: area 1 (zoom in 1.A) for which the proposed method detect no flood on November 3 and the DEM-fill method estimate a water elevation of 28 m; area 2 (zoom in 2.A) for which our method estimates a water level of 26.98 m and the fieldwork data 27.46 m (27.06 m elevation given by the DEM plus 0.4 m of flood depth estimated from fieldwork); area 3 (zoom in 3.A) for which our method detect no flood and the fieldwork data 27.45 m (27 m elevation given by the DEM plus 0.45 m of flood depth estimated from fieldwork). **Panel III** of Fig. 9 shows the flood extent derived with the DEM-fill method for different water levels: Fig. 9(d) with water level equal 26.98 m corresponding to the level estimated by our method; Fig. 9(e) with water level equal to 27.45 m, corresponding to the water level estimated by fieldwork data; Fig. 9(f) with water level equal to 28 m, corresponding to the level estimated by the DEM-fill method in order to obtain the same flood extent of the aerial photo.

Fig. 9(f) shows that with a water elevation of 28 m, based on the DEM we obtain a very similar water extent of the one observed in the aerial photo. If we set a water level of 27.45 m (Fig.(e)), the value estimated from fieldwork, we would obtain a slightly underestimated flood extent compared to the one observed in the aerial photo. From this analysis, we can estimate a water level on November 1 of 27.72 (average between 27.45 to 28 m).

Looking at Fig. 9(d), we can observe that the flood extent resulting with a water level of 26.98 m, the same estimated with our method, is very similar to the extent extracted from the SAR image. A similar extent confirms the goodness of the SAR-based flood map, while the estimation of the water level, 26.98 m, is comparable to the value estimated from the aerial photo and relative to 2 days before the SAR acquisition. This would mean a decrease of the water level of 0.74 m in two days. The reduction of flood extent in this area from November 2 to 3 is confirmed also by Radarsar-2 acquisition as we can see in Fig. 8a and b.

Nat. Hazards Earth Syst. Sci. Discuss., https://doi.org/10.5194/nhess-2018-158
Manuscript under review for journal Nat. Hazards Earth Syst. Sci.
Discussion started: 29 June 2018

Natural Hazards and Earth System Sciences
Discussions

Figure 9 Flood depth on November 3 over Ponti di Debba in the Vicenza area of interest; panel I shows (a) flood depth on the area analysed; (b) CSK image acquired on November 3 at 17:22 UTC from where the flood map has been derived; panel II shows (c) aerial view of the event acquired on November 1 at about 14:00 UTC with zooms on three areas (1.A, 2.A, 3.A) with relative fieldwork 410 **images (2.B and 3.B); panel III shows the flood extent derived with the DEM-fill method for different water levels: (d) with water level equal 26.98 m corresponding to the level estimated by the proposed method; (e) with water level equal to 27.45 m, corresponding to the water level estimated by fieldwork data; (f) with water level equal to 28 m, corresponding to the level estimated by the DEM-fill method in order to obtain the same flood extent of the aerial photo.**

In **Panel I** of Fig. 10, Fig. 10(a) shows flood extent and depth on November 3 at 17:22 UTC on the area of Via Isole, in the Saletto area, derived from the CSK SAR image shown in Fig. 10(b). **Panel II** of Fig. 10 shows aerial photo and fieldwork of the same area. Fig. 10(c) shows the aerial photo acquired on November 1 at about 14:50 UTC, where two areas are highlighted: area 1 (zoom in 1.A) for which the proposed method detects a water elevation of 11.6 m, the DEM-fill method estimates a water elevation of 11.4 m and the fieldwork data 11.38 m (10.7 m elevation given by the DEM plus 0.68 m of flood depth estimated from fieldwork).; area 2 (zoom in 2.A) for which the proposed method estimates a water elevation of 11.6 m and the fieldwork data 11.33 m (10.93 m elevation given by the DEM plus 0.4 m of flood depth estimated from fieldwork). **Panel III** of Fig. 10 shows the flood extent derived with the DEM-fill method for different water levels: Fig. 10(d) with water level equal to 11.6 m corresponding to the elevation estimated by the proposed method; Fig. 10(e) with water level equal to 11.38 m, corresponding to the water elevation estimated by field work; Fig. 10(f) with water level equal to 11.4 m, corresponding to the level estimated by the DEM-fill method in order to obtain the same flood extent of the aerial photo.

Fig. 10(f) shows that with a water elevation of 11.4 m, based on the DEM we obtain a very similar water extent of the one observed in the aerial photo. If we set a water level of 11.38 m (Fig. 10(e)), the value estimated from fieldwork, we would obtain the same flood extent compared to the one observed in the aerial photo. From this analysis, we can estimate a water level on November 1 of 11.38 m.

Looking at Fig. 10(d), we can observe that the flood extent resulting with a water level of 11.6 m, the same estimated with the proposed method, is very similar to the one observed in the SAR image.

Also in this case, an increase of 0.2 m from November 2 to 3 is consistent with the situation observed in from SAR acquisitions as shown in Fig. 8(c) and (d).

The same approach was followed for a total of 120 points distributed in the Vicenza (25 points) and Saletto area of study (95 points) as shown in Fig. 11. These points were selected based on recognizable features in the aerial or fieldwork photos of November 1 and 2. These points belonged to different flood polygons in the SAR-based flood map. For each point, we computed the difference between the water elevation estimated for November 1 or 2 based on aerial or fieldwork photos (step 1 of the assessment process) and the water elevation estimated from the SAR image for November 3. For the area of Vicenza we obtained an average difference of +53 cm. This difference is consistent with the observed change of flood depth (decrease) from November 1 and November 3. For the area of Saletto we obtained an average difference of -47 cm, a value that is consistent with the increase of flood depth observed from November 1 and November 3.

The differences are mainly due to the different timing of observation between the SAR image and the aerial and fieldwork photos. However, a source of errors is also intrinsic of the SAR method. In fact, we can have false alarms or false negative in the flood map (overestimation of flood extent due to radar shadow, or flood underestimation due to vegetation on top of flood areas) or misalignment between the DEM and the SAR data, which could be a geolocation error or an effect of different resolutions between the two datasets.

Nat. Hazards Earth Syst. Sci. Discuss., https://doi.org/10.5194/nhess-2018-158
Manuscript under review for journal Nat. Hazards Earth Syst. Sci.
Discussion started: 29 June 2018

Natural Hazards and Earth System Sciences
Discussions

Figure 10 Flood depth on November 3 over via Isole in the Saletto area of interest; panel I shows (a) flood depth on the area analysed; (b) CSK image acquired on November 3 at 17:22 UTC from where the flood map has been derived; panel II shows (c) aerial view of the event acquired on November 1 at about 14:50 UTC with zooms on two areas (1.A, 2.A) with relative fieldwork images (2.B and 3.B); panel III shows the flood extent derived with the DEM-fill method for different water levels: Fig. 10(d) with water level equal to 11.6 m corresponding to the elevation estimated by the proposed method; Fig. 10(e) with water level equal to 11.38 m, corresponding to the water elevation estimated by fieldwork for area 1; Fig. 10(f) with water level equal to 11.4 m, corresponding to the level estimated by the DEM-fill method in order to obtain the same flood extent of the aerial photo.

Nat. Hazards Earth Syst. Sci. Discuss., https://doi.org/10.5194/nhess-2018-158
Manuscript under review for journal Nat. Hazards Earth Syst. Sci.
Discussion started: 29 June 2018

Natural Hazards and Earth System Sciences
Discussions

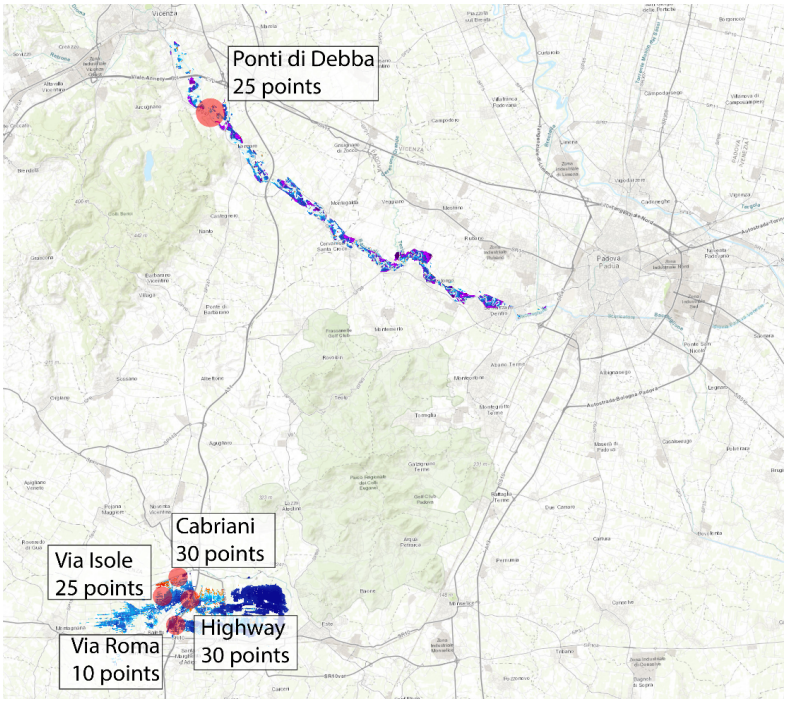

Figure 11 Overview of assessment points

5.2 Cross comparison: hydrodynamic modeling

Flood depth obtained with the presented methodology was compared with the one derived using a hydrodynamic model presented in Viero et al. (2013). The simulation was available for the area of Veggiano (area A1 in Fig. 3) and Bovolenta (area B in Fig. 3) on November 3 and 4 at the same time of the SAR acquisitions over the same areas. It made use of the DTM at 5 m resolution of the Veneto Region geodatabase, therefore the same DTM has been used with the proposed methodology to derive meaningful results for comparison.

The first row of Figure 12 shows the simulated flood depth (a), the SAR-based estimated flood depth (b) and the difference between the two (c) for Veggiano area on November 3, 2010. The second row, Fig. 12(d-f), shows the same series of results for the same area on November 4. The third row, Fig. 12(g-i), shows the same series of results for Bovolenta area on November 4.

Differences of two types can be seen between the two approaches: i) different flood extent and ii) different flood depth values between the model-based result and the SAR-based one. Concerning the first type of difference, Figure 13 shows the SAR image (a) from where the SAR-based flood extent (b) was derived and the flood extent derived by the hydrodynamic model (c). The red box in Fig. 13(b) and (c) delineates the boundary of the hydrodynamic modeling. From the comparison of these two extents, as well as the ones in Fig. 12, it is clear that the hydrodynamic model is overestimating the flood extent compared to the SAR observation. This leads to the second type of difference, *i.e.* the different values of flood depth. A different extent leads to a different estimation of the water surface, which in turn can be different depending on the methodology employed and therefore provides different flood depth value.

Analysing the two results, differences in flood extents seem to be the main driver of discrepancies. In fact, generally we can observe an overestimation of food depth by the hydrodynamic model, which is overestimating the flood extent. In the case

Nat. Hazards Earth Syst. Sci. Discuss., https://doi.org/10.5194/nhess-2018-158
Manuscript under review for journal Nat. Hazards Earth Syst. Sci.
Discussion started: 29 June 2018

Natural Hazards and Earth System Sciences
Discussions

of Veggiano on both dates (Fig. 12(c) and (f)), the difference is greater than 1 m only in small portion of the image (< 0.3 km^2), while in the rest of the image the difference in mainly between 10 and 50 cm. In the case of Bovolenta (Fig. 12(i)) the difference is bigger, with an area of about 1 km^2 with a difference greater than 1 m. In this case, we can also see an overestimation of depth by our method on the south east of the flood, which is almost in all the cases well below 1 m.

Table 2 and

Table 3 confirm this analysis. In fact, Table 2 compares the flood extent obtained by the model with the one derived from the SAR image showing the area reported only by the model, only by the SAR-based approach and the agreement between the two. If for the Veggiano area the difference between the two extents for both dates is limited to about 1 km^2, in the Bovolenta area the difference is more consistent, about 7 km^2, *i.e.* the model is reporting about two times the extent of the SAR observation. These numbers confirm the overestimation of the hydrodynamic model.

Table 3 instead compares numerically the flood depth obtained with the two methods. The Root Means Square Difference (RMSD) shows a value of 55 cm in the area of Veggiano on November 3, 73 cm on November 4 and a value of 79 cm in the area of Bovolenta on November 4. Once again, the numbers confirm the qualitative analysis and were expected given the overestimation of the flood extent by the model.

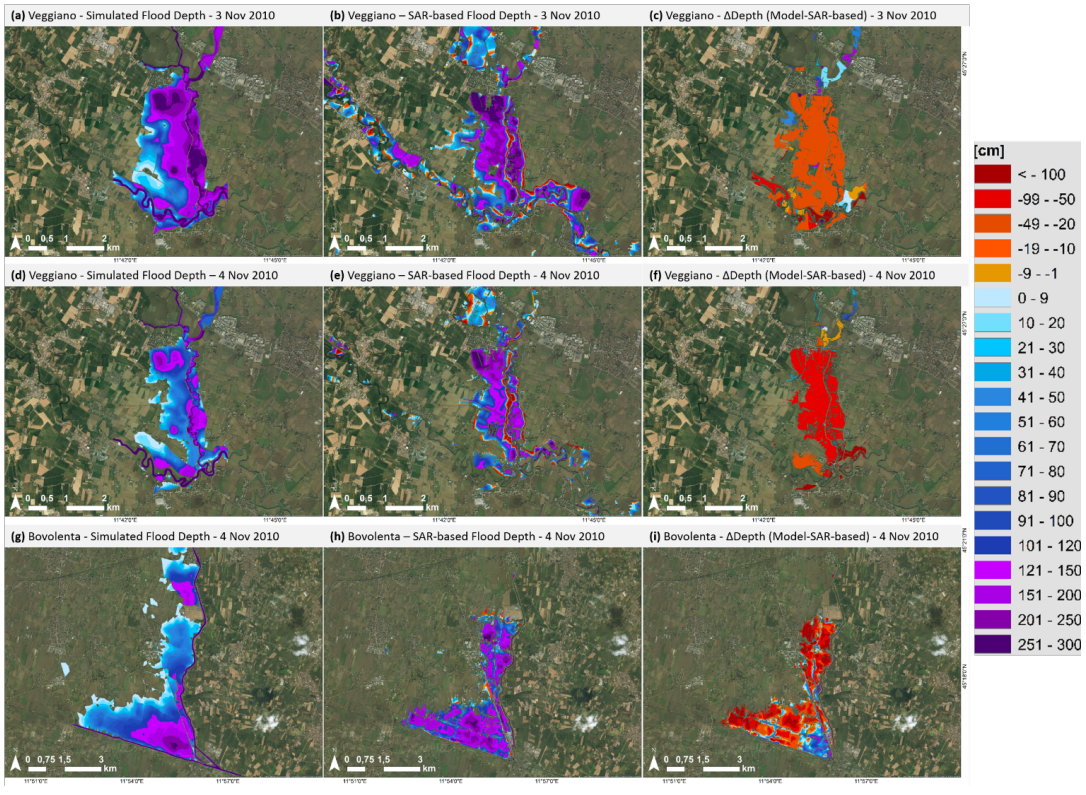

Figure 12 Comparison between the estimated flood extent and depth from hydrodynamic model and the proposed system based on the same DTM at 5 m resolution. (a-c): simulated flood depth, SAR-based flood depth and difference between the two for Veggiano area on November 3; (d-f): simulated flood depth, SAR-based flood depth and difference between the two for Veggiano area on November 4; (g-i): simulated flood depth, SAR-based flood depth and difference between the two for Bovolenta area on November 4.

Nat. Hazards Earth Syst. Sci. Discuss., https://doi.org/10.5194/nhess-2018-158
Manuscript under review for journal Nat. Hazards Earth Syst. Sci.
Discussion started: 29 June 2018

Natural Hazards and Earth System Sciences
Discussions

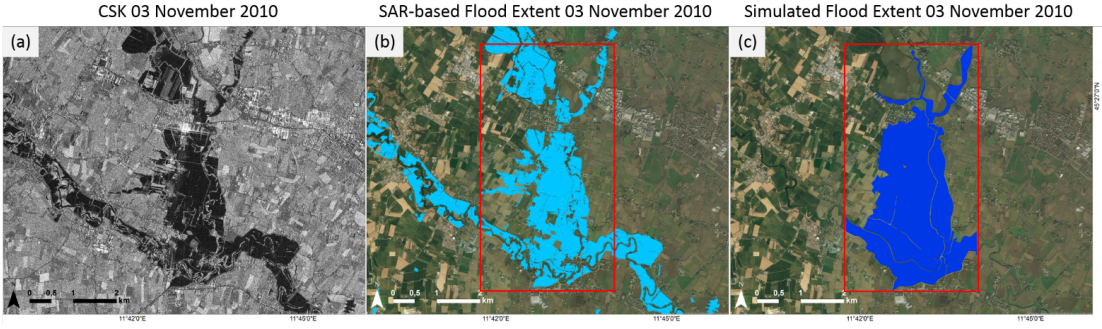

Figure 13 Comparison between SAR-based flood extent and simulated flood extent for the Veggiano area on November 3. (a) shows the CSK SAR image of November 3 2010; (b) shows the flood extent derived from the SAR image; (c) shows the simulated flood extent, which was calculated only for the area delimited by the red box. The difference between the two extents is very clear.

Table 2 Flood extent cross-comparison between SAR-based extent and hydrodynamic model-based extent.

Date - Area	Only hydrodynamic Model extent [km ^{2}]	Only SAR-based extent [km ^{2}]	Agreement between the two extents [Km^2]
3 Nov - Veggiano	6.81	5.86	4.33
4 Nov – Veggiano	4.87	3.82	2.77
4 Nov - Bovolenta	15.63	8.48	7.98

Table 3 Comparison between flood depth obtained with the hydrodynamic model and the proposed methodology

Date - Area	Mean Difference [cm]	Mean Absolute Difference [cm]	RMSD [cm]
3 Nov - Veggiano	-27	42	55
4 Nov – Veggiano	-63	68	73
4 Nov - Bovolenta	-37	62	79

6 Conclusions

In this paper, we showed a methodology for assessing flood depth based on a statistical analysis of elevation data along the boundary lines of flooded areas. Starting from flood extent maps and using high resolution DEM, water elevation can be estimated and therefore flood depth computed. The methodology may become suitable for operational mode. In fact, it meets the ideal requirements as indicated by Brown et al. (2016): accurate, simple to use also for non-GIS and RS experts, easily applicable to different satellite data (SAR and optical) and quick to apply.

The results have been assessed through aerial and fieldwork images acquired during the event. The assessment, carried out on 120 pints distributed in the area of Vicenza and Saletto, shows: i) an average underestimation of 53 cm for the area of Vicenza, due mainly to the decrease of water level from November 1 (date of aerial images) to November 3 (date of SAR acquisition); ii) an average overestimation of 47 cm, for the area of Saletto, due mainly to the increase of water level from November 1 (date of aerial images) to November 3 (date of SAR acquisition) in this part of the flood.

In comparison with hydrodynamic models, this methodology is more easily implemented since less information is needed: a stack of SAR images (before and after the event) and a DEM. Hydrodynamic models need additional information in order to derive depth, such as precipitation volumes, information about the soil, number and location of water pumps, etc.

520 The comparison with results obtained with a hydrodynamic model gives relatively good correspondence, the main difference being the different flood extent estimated by the model, which leads to a generally higher depth estimation. The model shows less accuracy together with a more complex utilization due to the additional data required to run it.

Despite the very good results obtained, the methodology can be further improved and automatized. Future work may consider to integrate a DEM filling procedure for improving water level estimation (Huang et al., 2014). The use of a vegetation
525 index such as NDVI, may be used to exclude wrong points along the boundary lines. In fact, in case vegetation is found along the boundary, that may indicate an error in the flood map and therefore the correspondent elevation would be an information to be discarded. Similarly, slope can be computed from the DEM and used to exclude errors due to radar shadow or misalignment between SAR and DEM data. In fact, in case the elevation measured is greater than a certain threshold, that may indicate that the point is on a steep area (e.g. river banks) and with high probability the point was wrongly included in the
530 flood map (radar shadow), or the pixel in the flood map does not exactly overlap the DEM. Excluding these possible sources of error would improve the statistics and therefore the estimation of the water level.

Moreover, shallow water in short vegetation could be mapped (Cian et al., 2018) and used to improve the SAR-based flood map from the omission errors caused by vegetation.

Another improvement may come from the method for creating the water elevation plane. Instead of relying simply on
535 the elevation values distribution, the plane that minimizes the RMSE could be found using the points on the boundary line left after the exclusion of outliers. The plane created could also take into consideration the slope of the river in a better way compared to the current method. By means of a shape index and the relative position between the river and the flooded area, the slope of the polygons can be estimated and imposed to the water plane. This would take into account the slope of the river and therefore the dynamics of the flood allowing to derive better results also for floods with a fast dynamic.

540 In conclusion, the proposed methodology shows great potential in support of rapid economic flood damage assessment. In fact, being able to rapidly estimate the flood depth, allows the computation of economic damage using available damage functions, which given a certain flood depth, returns the percentage of damage suffered by the economic asset considered. The precise estimation of flood depth value, increases the accuracy of the estimation of a flood impact, extremely important in the emergency response phase of a disaster.

545 **Acknowledgement**

The authors would like to thank the Italian Space Agency (ASI), which provided the SAR data for producing the flood maps, A. Metz, German Aerospace Center, who provided support to write the script in Python, D. P. Viero, University of Padua, which kindly provided the hydrodynamic modeling of the event and support in evaluating our results and M. Martone, German Aerospace Center for the precious comments and suggestions that helped improving this work.

550 **References**

Amadio, M., Mysiak, J., Carrera, L., & Koks, E. (2016). Improving flood damage assessment models in Italy. *Natural Hazards*, *82*(3), 1–14. http://doi.org/10.1007/s11069-016-2286-0

ArcPy. http://pro.arcgis.com/en/pro-app/arcpy/get-started/what-is-arcpy-.htm

ARPAV (2010). SCHEDA EVENTO " PLUVIO ", (Figura 2), 1–16.

555 Brown, K. M., & Brownett, J. M. (2016). Progress in operational flood mapping using satellite synthetic aperture radar (SAR) and airborne light detection and ranging (LiDAR) data. http://doi.org/10.1177/0309133316633570

Carrera, L., Standardi, G., Bosello, F., & Mysiak, J. (2013). Assessing direct and indirect economic impacts of a flood event

through the integration of spatial and computable general equilibrium modelling. *CMCC Research*, *63*, 1–27. http://doi.org/10.1016/j.envsoft.2014.09.016

Cian, F., Marconcini, M., & Ceccato, P. (2018). Normalized Difference Flood Index for rapid flood mapping: Taking advantage of EO big data. *Remote Sensing of Environment*, *209*(March), 712–730. http://doi.org/10.1016/j.rse.2018.03.006

Cohen (1968). WEIGHTED KAPPA. *Psychological Bulletin*, 257–72. Retrieved from http://www.ncbi.nlm.nih.gov/pubmed/19586159

D'Alpaos, L., Brath, A., & Fioravante, V. (2014). Relazione tecnico-scientifica sulle cause del collasso dell ' argine del fiume Secchia avvenuto il giorno 19 gennaio 2014 presso la frazione San Matteo.

European Commission (2007). Directive 2007/60/EC of the European Parliament and of the Council. *Official Journal of the European Union*, *288*(2455), 27–34. http://doi.org/English

Copernicus EMS. Copernicus Emergency Management Service. Retrieved from http://emergency.copernicus.eu/mapping/copernicus-emergency-management-service

Floris, M., D'Alpaos, A., De Agostini, A., Stevan, G., Tessari, G., & Genevois, R. (2012). A process-based model for the definition of hydrological alert systems in landslide risk mitigation. *Natural Hazards and Earth System Science*, *12*, 3343–3357. http://doi.org/10.5194/nhess-12-3343-2012

Franceschetti, G., & Lunari, R. (2018). *Synthetic aperture radar processing*. CRC press.

Giustarini, L., Hostache, R., Matgen, P., Schumann, G. J., Bates, P. D., & Mason, D. C. (2013). A Change Detection Approach to Flood Mapping in Urban Areas Using TerraSAR-X. *IEEE Transactions on Geoscience and Remote Sensing*, *51*(4), 2417–2430. http://doi.org/10.1109/TGRS.2012.2210901

Giustarini, L., Vernieuwe, H., Verwaeren, J., Chini, M., Hostache, R., Matgen, P., … De Baets, B. (2015). Accounting for image uncertainty in SAR-based flood mapping. *International Journal of Applied Earth Observation and Geoinformation*, *34*, 70–77. http://doi.org/10.1016/j.jag.2014.06.017

Gupta, R. P., & Banerji, S. (1985). Monitoring of reservoir volume using LANDSAT data. *Journal of Hydrology*, *77*(1–4), 159–170. http://doi.org/10.1016/0022-1694(85)90204-5

Henry, J. B., Chastanet, P., Fellah, K., & Desnos, Y. L. (2006). Envisat multi-polarized ASAR data for flood mapping. *International Journal of Remote Sensing*, *27*(9–10), 1921–1929. http://doi.org/Doi 10.1080/01431160500486724

Huang, C., Chen, Y., Wu, J., Chen, Z., Li, L., Liu, R., & Yu, J. (2014). Integration of remotely sensed inundation extent and high-precision topographic data for mapping inundation depth. *2014 The 3rd International Conference on Agro-Geoinformatics, Agro-Geoinformatics 2014*, 1–4. http://doi.org/10.1109/Agro-Geoinformatics.2014.6910580

Iervolino, P., Guida, R., Iodice, A., & Riccio, D. (2015). FloodingWater Depth Estimation With High-Resolution SAR, *53*(5), 2295–2307.

International Charter. International Charter on Space and Major Disasters. Retrieved from https://www.disasterscharter.org

Long, S., Fatoyinbo, T. E., & Policelli, F. (2014). Flood extent mapping for Namibia using change detection and thresholding with SAR. *Environmental Research Letters*, *9*(3), 035002. http://doi.org/10.1088/1748-9326/9/3/035002

Martinis, S., Kersten, J., & Twele, A. (2015). A fully automated TerraSAR-X based flood service. *ISPRS Journal of Photogrammetry and Remote Sensing*, *104*, 203–212. http://doi.org/10.1016/j.isprsjprs.2014.07.014

Martinis, S., Twele, a., & Voigt, S. (2009). Towards operational near real-time flood detection using a split-based automatic thresholding procedure on high resolution TerraSAR-X data. *Natural Hazards and Earth System Science*, *9*(2), 303–314. http://doi.org/10.5194/nhess-9-303-2009

Mason, D. C., Davenport, I. J., Flather, R. a., Gurney, C., Robinson, G. J., & Smith, J. a. (2001). A Sensitivity Analysis of the Waterline Method of Constructing a Digital Elevation Model for Intertidal Areas in ERS SAR scene of Eastern England.

600 *Estuarine, Coastal and Shelf Science*, *53*(6), 759–778. http://doi.org/10.1006/ecss.2000.0789

Matgen, P., Giustarini, L., Chini, M., Hostache, R., Wood, M., & Schlaffer, S. (2016). Creating a water depth map from SAR flood extent and topography data. *International Geoscience and Remote Sensing Symposium (IGARSS)*, *2016–Novem*, 7635–7638. http://doi.org/10.1109/IGARSS.2016.7730991

Matgen, P., Schumann, G., Henry, J.-B., Hoffmann, L., & Pfister, L. (2007). Integration of SAR-derived river inundation
605 areas, high-precision topographic data and a river flow model toward near real-time flood management. *International Journal of Applied Earth Observation and Geoinformation*, *9*(3), 247–263. http://doi.org/10.1016/j.jag.2006.03.003

Mojtahed, V., Giupponi, C., Biscaro, C., Gain, A. K., & Balbi, S. (2013). Integrated Assessment of Natural Hazards and Climate Change Adaptation : II . The SERRA Methodology, (07).

MunichRE. (2014). *Loss events worldwide 2014 Percentage distribution*.

610 Mysiak, J., & Luther, J. (2013). Towards a potential European flood impact database. EEA – JRC – ETC/CCA Joint Technical Paper.

O'Grady, D., Leblanc, M., & Gillieson, D. (2011). Use of ENVISAT ASAR Global Monitoring Mode to complement optical data in the mapping of rapid broad-scale flooding in Pakistan. *Hydrology and Earth System Sciences*, *15*(11), 3475–3494. http://doi.org/10.5194/hess-15-3475-2011

615 Oberstadler, R., H??nsch, H., & Huth, D. (1996). Assessment of the mapping capabilities of ERS-1 SAR data for flood mapping: A case study in Germany. *European Space Agency, (Special Publication) ESA SP*, *11*(383), 247–252. http://doi.org/10.1002/(SICI)1099-1085(199708)11:10<1415::AID-HYP532>3.0.CO;2-2

Pierdicca, N., Pulvirenti, L., Chini, M., Guerriero, L., & Candela, L. (2013). Observing floods from space : Experience gained from COSMO-SkyMed observations. *Acta Astronautica*, *84*, 122–133. http://doi.org/10.1016/j.actaastro.2012.10.034

620 Schumann, G., Hostache, R., Puech, C., Hoffmann, L., Matgen, P., Pappenberger, F., & Pfister, L. (2007). High-resolution 3-D flood information from radar imagery for flood hazard management. *IEEE Transactions on Geoscience and Remote Sensing*, *45*(6), 1715–1725. http://doi.org/10.1109/TGRS.2006.888103

Schumann, G. J., Neal, J. C., Mason, D. C., & Bates, P. D. (2011). Remote Sensing of Environment The accuracy of sequential aerial photography and SAR data for observing urban fl ood dynamics , a case study of the UK summer 2007 fl oods.
625 *Remote Sensing of Environment*, *115*(10), 2536–2546. http://doi.org/10.1016/j.rse.2011.04.039

Schumann, G., Matgen, P., Cutler, M. E. J., Black, A., Hoffmann, L., & Pfister, L. (2008). Comparison of remotely sensed water stages from LiDAR, topographic contours and SRTM. *ISPRS Journal of Photogrammetry and Remote Sensing*, *63*(3), 283–296. http://doi.org/10.1016/j.isprsjprs.2007.09.004

Scorzini, A. R., & Frank, E. (2015a). Flood damage curves : new insights from the 2010 flood in Veneto , Italy, 1–12.
630 http://doi.org/10.1111/jfr3.12163

Scorzini, A. R., & Frank, E. (2015b). Flood damage curves: New insights from the 2010 flood in Veneto, Italy. *Journal of Flood Risk Management*, 1–12. http://doi.org/10.1111/jfr3.12163

UNIDSR. (2015). *Making Development Sustainable: The Future of Disaster Risk Management. Global Assessment Report on Disaster Risk Reduction*.

635 Viero, D. P., Peruzzo, P., Carniello, L., & Defina, A. (2014). Integrated mathematical modeling of hydrological and hydrodynamic response to rainfall events in rural lowland catchments. *Water Resources Research*, *50*(7), 5941–5957. http://doi.org/10.1002/2013WR014293

Viero, D. Pietro, D'Alpaos, A., Carniello, L., & Defina, A. (2013). Mathematical modeling of flooding due to river bank failure. *Advances in Water Resources*, *59*, 82–94. http://doi.org/10.1016/j.advwatres.2013.05.011

640 Zollo, A. L., Rillo, V., & Bucchignani, E. (2015). Extreme temperature and precipitation events over Italy : assessment of high-resolution simulations with COSMO-CLM and future scenarios. http://doi.org/10.1002/joc.4401

Zwenzner, H., & Voigt, S. (2008). Improved estimation of flood parameters by combining space based SAR data with very high resolution digital elevation data. *Hydrology and Earth System Sciences Discussions*, *5*, 2951–2973. http://doi.org/10.5194/hessd-5-2951-2008

645